DOI 10.24425/aee.2023.143689

Analysis of the operation of a switched reluctance motor in the extended constant power range

MARIUSZ KORKOSZ ✉, GRZEGORZ PODSKARBI, KRYSTYNA KRZYWDZIŃSKA-KORNAK

Faculty of Electrical and Computer Engineering
Rzeszow University of Technology
Al. Powstańców Warszawy 12, 35-959 Rzeszów, Poland
e-mail: {✉mkosz/g.podskarbi/krzywdzinska}@prz.edu.pl

(Received: 11.06.2022, revised: 29.09.2022)

Abstract: In this paper, an analysis of the properties of a switched reluctance motor (SRM) 8/6 in an extended constant power range is presented. The typical constant power range to constant torque range ratio is between 2 and 3. In the case of machines designed as an electric vehicle drive, it is important to maximize this ratio. In the case of an SRM, it is possible to achieve this by applying an appropriate control strategy. An analysis of the SRM operation utilizing a modified control algorithm allows control of the maximum value of the motor phase current. As a consequence, using the so-called nonzero initial conditions for the current and flux allows the output power to be maintained in a wide speed range. For the improvement of drive system efficiency, the work of the phase current regulator should be limited to a minimum. The most advantageous work conditions we obtain with single-time current regulator work. Laboratory verification has been performed for selected states of motor work.

Key words: continuous conduction, control strategy, extended constant power range, SRM, switched reluctance motor

1. Introduction

Most electrical machines can be used as the main drive in electric and hybrid vehicles [1–3]. In this case, the constant power (CP) range to constant torque (CT) range ratio (CP/CT) is significant. At the same time, for many years, there has been a tendency to use a brushless permanent magnet motor (BLPM) in this drive [3–7]. However, the uncertain political situation, increasing prices of magnets, and monopolized production are causes for seeking an alternative solution. In a range of drives with a CP/CT ratio bigger than 2, an induction motor, a classical synchronous

motor, and switched reluctance motor can be applied [2, 3, 8–10]. The CP/CT range of work is also essential in the case of light vehicles [11], starter-generator systems [12], or even, e.g. bicycles [13, 14]. The CP/CT ratio depends on the machine type and varies from 1 (brushless DC motor – BLDCM) to 5 (induction motor – IM) [15]. It is also possible to extend the CP range of the BLDCM by modifying the design. Nevertheless, the cost of production of these motors is increasing. The cheapest and easiest solution that we can use in the drive system is a switched reluctance motor. Its typical CP/CT ratio is approximately 3 and depends on the number of phases and construction parameters (width of the stator and rotor poles) [16]. Using wider stator and rotor poles is beneficial for decreasing the electromagnetic torque ripple. At the same time, it decreases the CP/CT ratio. In practice, it is essential to achieve a trade-off between the CP/CT ratio and the value of electromagnetic torque ripple.

The typical CP/CT ratio equal to 3 is a satisfactory value. These values are obtained by using the classical control method of a switched reluctance motor. In a classical single-pulse control, zero initial conditions for the phase current are assumed. Thus, the control parameters are limited.

In the literature, the analysis of an operation of the switched reluctance motor with nonzero initial conditions is presented [16–21]. This is the so-called continuous conduction mode (CC). The authors of [17–21] indicate that constant conduction can be used in the range of constant power. The CP range can be extended by utilizing a continuous conduction mode.

In this paper, an analysis of the operation of the switched reluctance motor in an extended constant power range is presented. To obtain the output power in continuous conduction mode, the turn-on angle, turn-off angle, and reference current control are proposed. According to the authors, a change in the control algorithm within a constant conduction range allows one to achieve very effective motor operation. Maintaining the preset output power in the CC range can be achieved by controlling the maximum value of the phase current in the current control range with the minimization of the number of switching events of the current regulator. The salient rotor poles construction forces air flow. Thus, the rotor acts as an internal fan. During work in a range of constant power (high speed), the cooling of the stator winding is more effective. On the other hand, salient pole rotor construction increases windage loss. Under laboratory conditions, a motor test was performed in a range of continuous conduction.

2. Analyzed design

The object of the study was a four-phase switched reluctance motor 8/6. This is a commercial construction. In Fig. 1, a view of the motor and simplified cross-section of the stator and the rotor.

In Table 1, the selected nominal parameters of the analyzed construction are presented.

The static characteristics of the electromagnetic torque $T_e = f(\theta)$ is presented in Fig. 2. In laboratory conditions, the value of the phase current has been changed to 80 A, with the level of value being 10 A. Laboratory tests have been done only for three current values, i.e. I = 10 A, 20 A and 30 A.

Satisfactory compatibility of numerical calculations and the laboratory test has been achieved. Some difference is visible with the rotor position angle above 20°. In laboratory conditions, a lower value of the manufactured electromagnetic torque occurred. The reason is the greater state of stator electromagnetic circuit saturation.

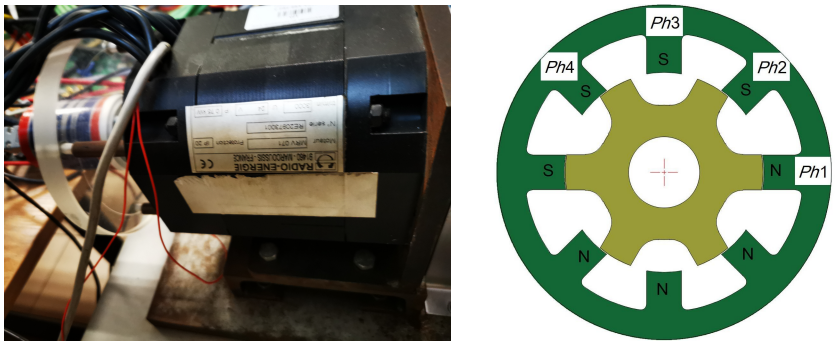

(a) (b)

Fig. 1. Analyzed construction view (a); geometrical cross-section of the stator and the rotor (b)

Table 1. Selected nominal parameters analysis of SRM 8/6

Parameter	**Value**	**Unit**
Nominal voltage U_{dc}	24	V
Nominal power P_N	750	W
Nominal speed n_N	3 000	rpm
Locked rotor torque T_s	13	N·m
Number of stator poles N_s	8	–
Number of rotor poles N_r	6	–
Stator pole arc β_s	19	°
Rotor pole arc β_r	20	°
Maximum DC current $I_{\mathrm{dc\,max}}$	150	A
Maximum efficiency η_{max}	80	%
Maximum speed n_{max}	4 000	rpm

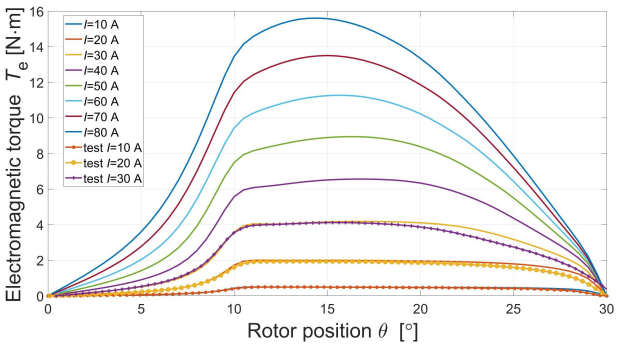

Fig. 2. Electromagnetic torque vs. rotor position at I = var

The torque vs. speed characteristics of the analyzed design is presented in Fig. 3 (designated by the manufacturer).

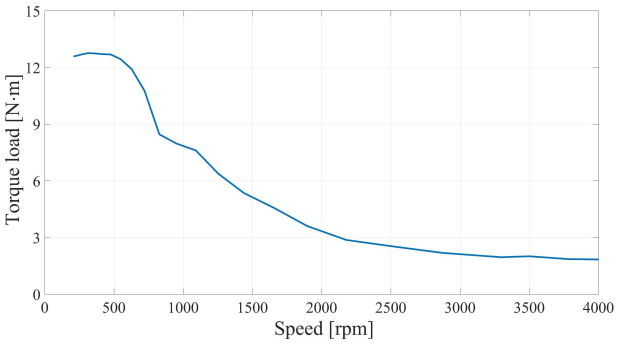

Fig. 3. Mechanical characteristics of the analyzed construction

The range of constant torque in the tested motor occurs at a speed of about 650 rpm. Above that speed, the motor works with constant power. The range of CP/CT for the factory regulator is above 6. In a laboratory system, the maximum phase current value was limited to 75 A. The manufacturer limited the maximum motor speed to 4 000 rpm. In the authors opinion, factory controller software limits do not allow the motor output power to be increased over 3 000 rpm. It is possible not only to increase the output power but also to extend the range of work to constant power (CP) by modification of the control algorithm.

3. Control focused on overlong range of constant power

In a typical control for a switched reluctance motor, it is assumed that the initial current is equal to zero (before the next electric period). This means that the motor phase is in a current-less state. In Fig. 4, the theoretical self-inductance and current waveforms (single-pulse control) are presented.

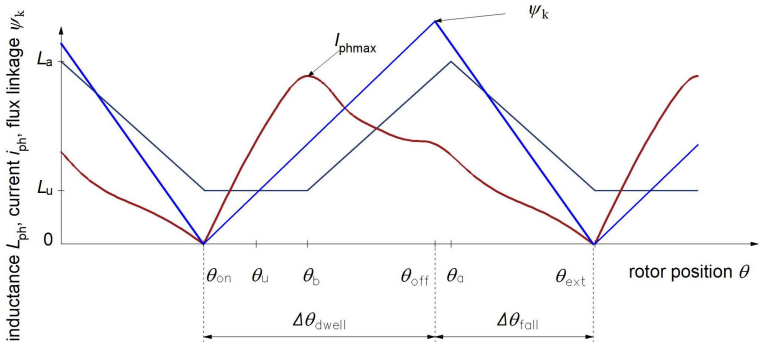

Fig. 4. Idealized self-inductance L_{ph}, flux linkage ψ_{ph}, and phase current i_{ph} vs the rotor position for single pulse control

The angle at which the current decay occurs is marked as θ_{ext}, the turn-on angle as θ_{on}, turn-off angle θ_{off}, conduction angle $\Delta\theta_{\text{dwell}}$, and decay angle $\Delta\theta_{\text{fall}}$. The minimum inductance occurs at the angle θ_u, while the maximum inductance occurs at the angle θ_a. The angle θ_b is defined as the first edge position. It is determined from the dependence [16]:

$$\theta_b = \frac{180}{N_r} - \frac{(\beta_s + \beta_r)}{2}. \tag{1}$$

With the angle θ_b in the range of single-pulse control, the current reaches the maximum value $I_{\text{ph max}}$ (when forcing the excitation which is using in the range of CP work).

For single-pulse control, the current decreases to zero before the next turn on of a given strand (Fig. 4). Fulfillment of this condition is synonymous to zero initial conditions for the phase current for the next electrical cycle and allows implementation of a control strategy focused on efficiency optimization. The range of constant power control depends on the geometric dimensions of the stator and rotor poles. A wider range of constant power is obtained for smaller values of the stator and rotor pole arcs. However, this causes an increase in the electromagnetic torque ripple. Increasing the pole arc of the stator and the rotor pole reduces electromagnetic torque ripple. It must be understood that the influence of the arc of the stator and the rotor pole is important for the range of work with constant power. The stator and rotor poles arc influences on the value of angle θ_b (equation (1)). Decreasing the angle θ_b value affects the range of work with constant power (CP).

The nonzero initial conditions for the phase currents have an important effect on the output power possible. In Fig. 5, idealized waveforms for the continuous conduction state are presented.

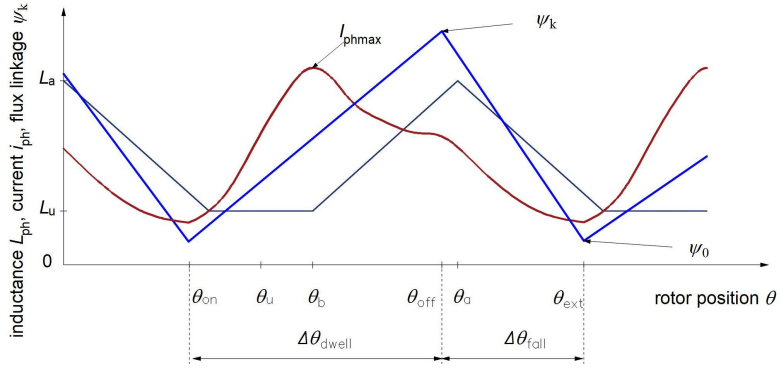

Fig. 5. Idealized self-inductance, flux linkage and phase current vs the rotor position for continuous conduction

The motor control algorithm must limit the dwell angle for continuous conduction. The theoretical value of the dwell angle defines the geometry of the motor (omitting copper loss and converter loss):

$$\Delta\theta_{\text{dwell\_}t} = \frac{180}{N_r}. \tag{2}$$

In fact, the maximum value of the dwell angle depends on the voltage drop Δu_+ (on the winding resistance and transistors) and diodes Δu_-.

The approximate maximum dwell angle value determines the equation (omitting the influence of the winding temperature and power electronic devices) [16]:

$$\Delta\theta_{\text{dwell\_max}} = \Delta\theta_{\text{dwell\_}t}\frac{1+\Delta u_-}{2-\Delta u_+ + \Delta u_-}\,. \tag{3}$$

For the control strategy, a limited dwell angle value is important. A control algorithm focused on an increase of output power must take into account the dwell angle value greater than $\Delta\theta_{\text{dwell\_max}}$.

The turn on angle θ_{on} required to obtain the maximum current value $I_{\text{ph max}}$ can be approximately calculated with the equation [16]:

$$\theta_{\text{on}} = \theta_b - L_u\omega\frac{I_{\text{ph max}}}{U_{\text{dc}}}\,, \tag{4}$$

where ω is the angular rotor speed.

Equation (3) allows us to estimate the value of the turn-on angle in the range of single-pulse control. In the range of continuous conduction, the turn on angle value depends on the maximum phase current value and the dwell angle value because of the nonzero initial conditions.

The output power can be controlled by changing the reference maximum phase current $I_{\text{ph max}}$. To control the maximum phase current value, a hysteresis controller could be used. To provide a high efficiency of energy conversion, it is advisable to minimize the switching events of the current controller. In that case, the smallest RMS of the phase current is obtained.

4. The results of numerical calculation

Calculations were performed on the basis of the numerical model. In Fig. 6, the process of the motor entering into a state of continuous conduction (flux linkage vs current) with speed 3 000 rpm.

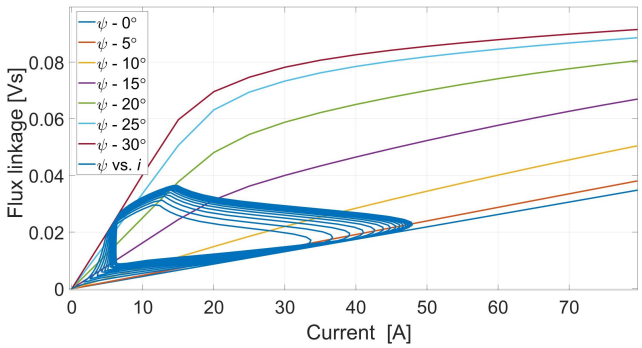

Fig. 6. Flux linkage vs current (based on flux characteristics)

In a state of continuous conduction, the phase current can reach much greater maximum values. This causes a much larger energy flow. It consequently results in the growth of generated

electromagnetic torque and output power. Control of the maximum current value is important not only for the regulation of the output power value. The lack of control of the maximum current value can provide an excessive increase in output power. In Fig. 7 the calculated electromagnetic torque T_e (Fig. 7(a)) and the output power (Fig. 7(b)) vs. the rotational speed are presented. In the calculations, we assumed that the current controller limited the maximum phase current value $I_{\text{ph max}}$.

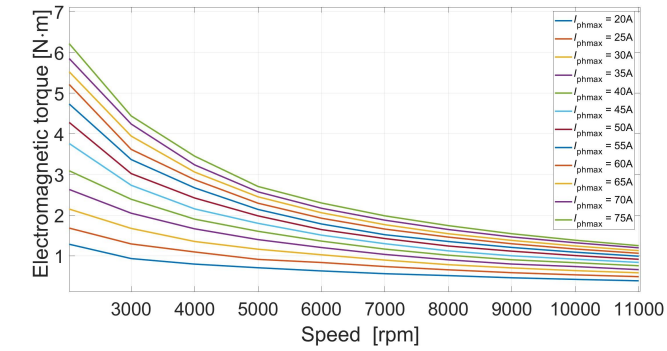

(a)

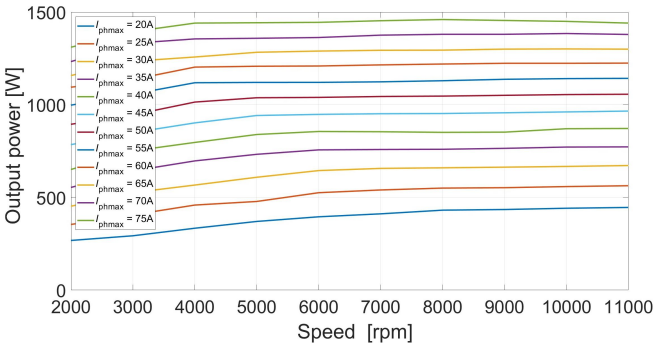

(b)

Fig. 7. Electromagnetic torque vs. speed (a); and output power vs. speed (b) at $I_{\text{ph max}}$ = var

Because of the simultaneous control of the angles and maximum phase current value, the range of CP can be extended. The dependence between the output power and the maximum phase current value is almost linear. In Fig. 8, the control angle vs. rotational speed characteristics is presented.

In the range of CC angles, the angles change slightly. Increasing the maximum phase current value from 35 A to 70 A forced an increase of the turn on angle to approximately 7° el. (1.17° mech.). The dwell angle increased to approximately 6° el. (1° mech.). In a real system, this requires the use of high-resolution encoders. The change in the turn-on and conduction angles in a measure is dependent on the required maximal current value. This is connected to an owned motor self-inductance profile.

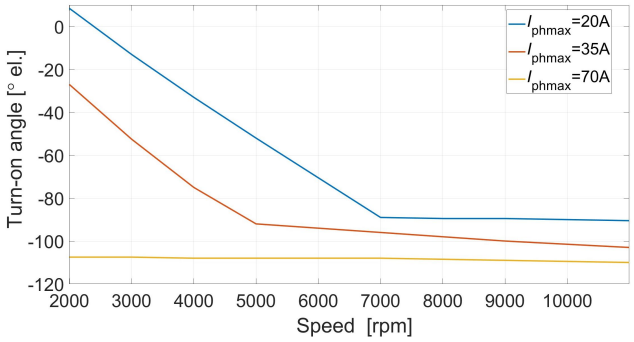

(a)

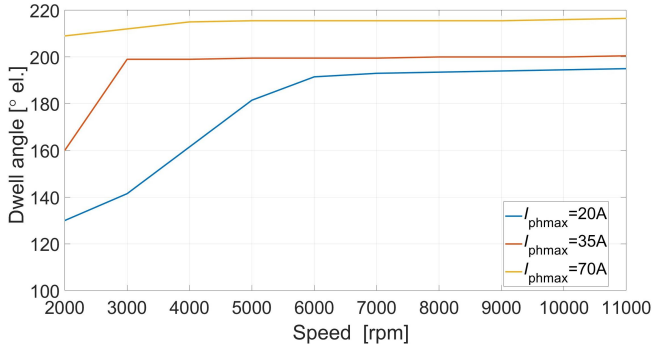

(b)

Fig. 8. Turn-on angle vs speed (a); and dwell angle vs speed (b) at $I_{\text{ph max}}$ = var

Widening the range of constant power using the CC method affects the increasing electromagnetic torque ripple in a negative way. Figure 9(a) shows an exemplary electromagnetic torque vs. time in a range of constant conduction with $I_{\text{ph max}}$ = 40 A with the minimalization of switching the regulator (Fig. 9(b)). In the numerical model, excitation of selected stator poles e.g.: NSSSSNNN has been used (Fig. 1(b)). Figure 9(a) shows the components of the electromagnetic torque. The waveforms of phase currents and corresponding them electromagnetic phase torques have been determined in the absence of magnetic couplings (MCs).

The motor electromagnetic torque (Fig. 9(a)), despite the control symmetry and the numerical model, is not a symmetrical course. It appears because in the range of CC, phase current flows all the time, so the influence of magnetic coupling (MC) is much greater. This one affects the increasing electromagnetic torque ripple. Widening the range of constant power by using the CC method affects the increasing electromagnetic torque ripple in a negative way. Fig. 9(a) shows an exemplary electromagnetic torque vs the rotor position in a range of constant conduction with $I_{\text{ph max}}$ = 40 A with the minimalization the switching phase current regulator (Fig. 9(b)). It causes a decrease in the copper losses. Therefore, it allows increasing the efficiency of drive in the range of CC.

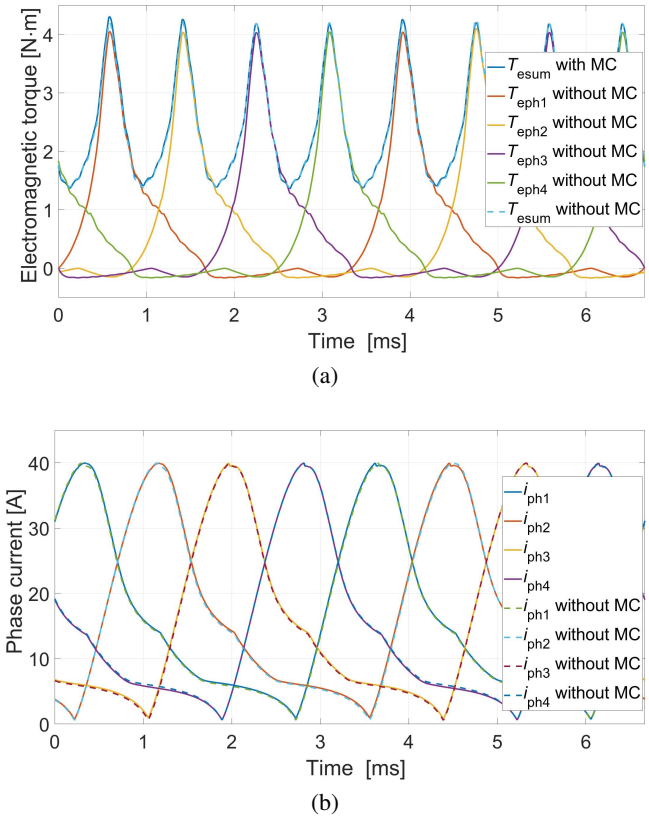

Fig. 9. Typical continuous conductions at 3 000 rpm waveform of electromagnetic torque (a); waveforms of phase current (b)

The characteristics presented in Fig. 8 have been calculated without thermal limitations and mechanical loss. In a real system, obtaining an output power above 750 W, e.g. with a speed equal to 11 000 rpm, should be treated as overload. In Fig. 10 an exemplary motor temperature distribution with a speed equal to 11 000 rpm and $I_{\mathrm{ph\,max}} = 35$ A is presented.

In the case of work with nominal power with a speed of 11 000 rpm (Fig. 9), the maximal temperature (equal to 147.17°C) has been obtained. It allows for the constant work of motor. Worktime in the range of overload depends on the actual winding temperature. When a motor works with nominal power, e.g. with a speed of 11 000 rpm, the increase in output power is possibly only possible for a few seconds. In Fig. 11 the winding temperature vs. time with a speed equal to 11 000 rpm and current increases to $I_{\mathrm{ph\,max}} = 70$ A is presented.

In the state of double overload, the maximal temperature of the stator is reached at about 32 seconds (Fig. 11). After that time, the motor load has to be reduced to a nominal value.

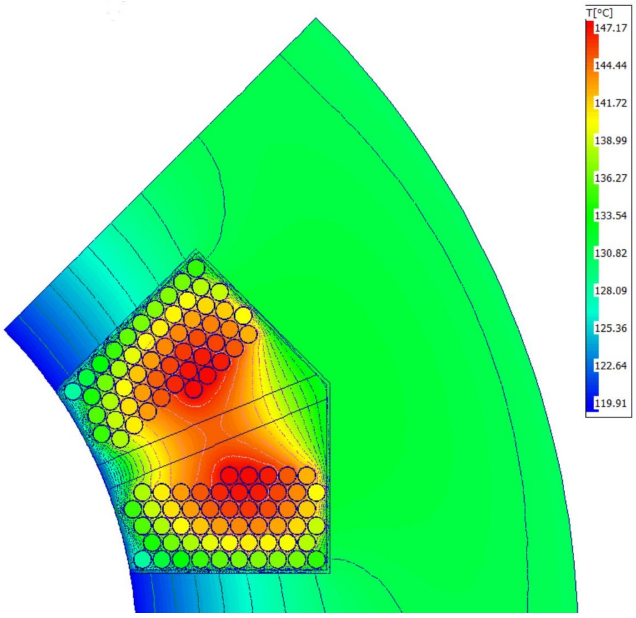

Fig. 10. The temperature distribution with speed equals 11 000 rpm and $I_{\text{ph max}}$ = 35 A

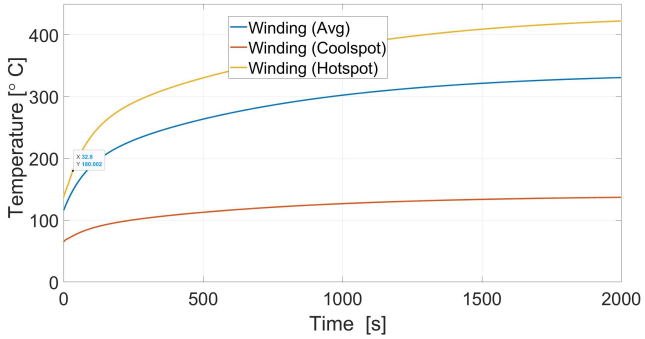

Fig. 11. The winding temperature vs. time with speed equal to 11 000 rpm and current increased to $I_{\text{ph max}}$ = 70 A

5. Laboratory tests

The tests were performed under laboratory conditions. For the selected control parameters, torque vs. speed and overall efficiency characteristics were obtained. Current waveforms in the range of continuous conduction were registered. In Fig. 12 a block diagram of the laboratory stand is presented.

As a load, a Magtrol PB43 dynamometer was used. It can operate up to about 4 000 rpm. For this reason, only a partial verification in the CP range was performed.

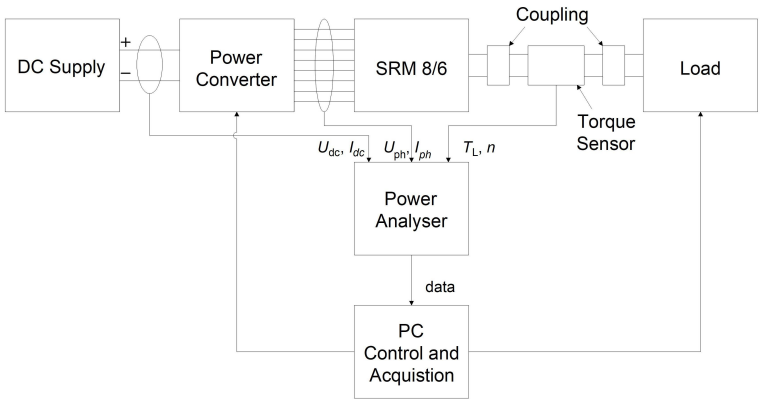

Fig. 12. Block diagram of the measuring system

In Fig. 13 the current waveforms for a speed equal to 3 000 rpm are presented. Due to the encoder resolution, the waveforms in Fig. 13 were designated with the same turn-off angle (120°). The turn-on angle was changed every 3°. The results of numerical calculation have been placed on Fig. 13 (for the same control conditions).

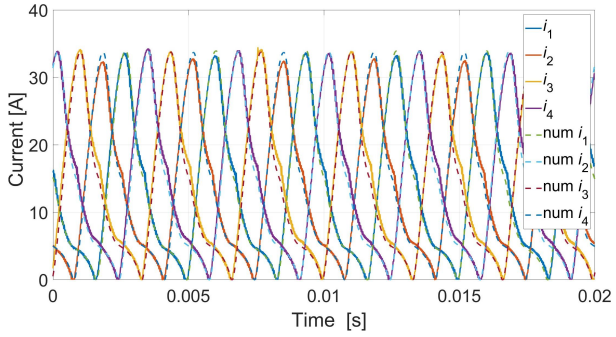

(a)

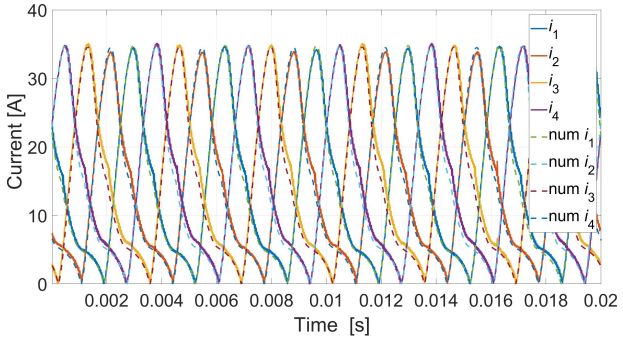

(b)

Fig. 13

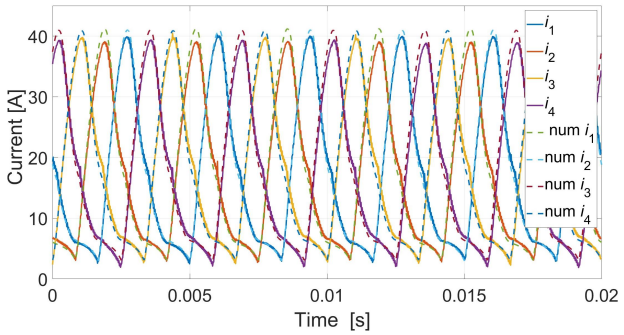

(c)

Fig. 13. Exemplary current waveforms at a rotor speed of n = 3 000 rpm single pulse control ($\Delta\theta_{\text{dwell}} < \Delta\theta_{\text{dwell\_max}}$) (a); with a limit of single pulse control ($\Delta\theta_{\text{dwell}} = \Delta\theta_{\text{dwell\_max}}$) (b); and continuous conduction ($\Delta\theta_{\text{dwell}} > \Delta\theta_{\text{dwell\_max}}$) (c)

Under laboratory tests, there are visible differences between different phase currents. These are caused by technical differences and magnetic couplings between phases [18]. In the real system, the electromagnetic torque ripple will be even greater than in the numerical tests (Fig. 9(a)). In real system in individual currents waveforms they are much bigger differences between them.

The measured characteristics of load torque, output power, overall efficiency, and current value vs. speed are presented in Figs. 14–18. The results of laboratory tests have been related to selected numerical tests (at n = 1 800 rpm, 3 000 rpm and 4 000 rpm). The numerical tests have been done for the same control parameters.

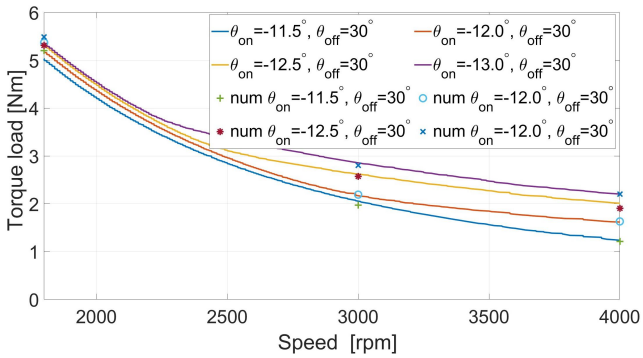

Fig. 14. Torque load vs. speed – laboratory test

Laboratory tests carried out in a limited range confirm the possibility of an extension of the CP range. Obtaining output power in a wide range of values is possible. The results of laboratory tests confirmed that the CC control method is highly sensitive to the control parameters. In laboratory conditions, some efficiency of drive system improvement (82% with 4 000 rpm) has been obtained because of the nullify conduction angle maximal value limitation. Simultaneously the transition

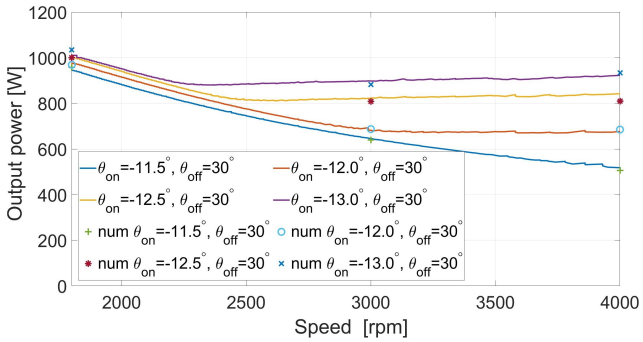

Fig. 15. Output power vs. speed – laboratory test

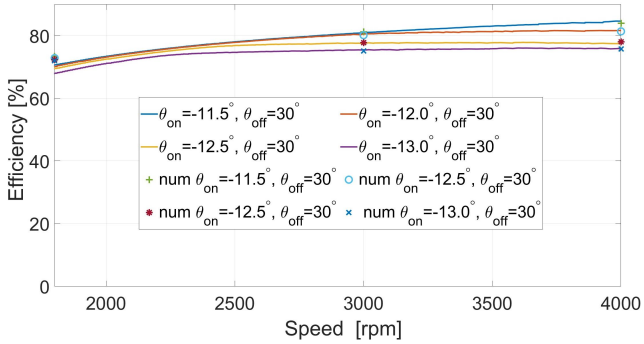

Fig. 16. Overall efficiency vs. speed – laboratory test

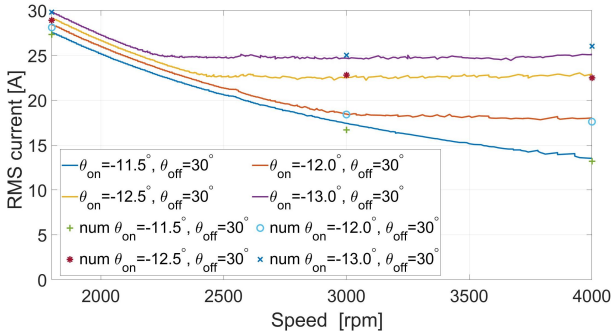

Fig. 17. RMS current vs. speed – laboratory test

in CC state is not increasing in the drive system (Fig. 16). The results of laboratory tests indicate that to maintain CC with the current amplitude value which is given enough output power is acceptable (Fig. 18). It allows essentially increasing the range of rotation speed regulation. The effective value (Fig. 17) and the amplitude (Fig. 18) of current with the CC control for the

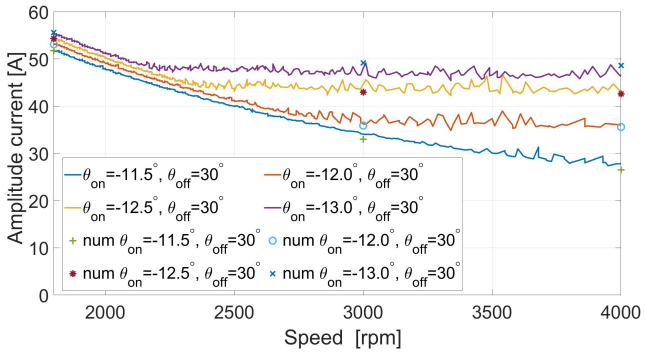

Fig. 18. Amplitude current vs. speed rotation – laboratory test

described parameters have been obtained at a practically constant level. This confirms the result of the numerical test (Fig. 7(b)) in the range of ability of regulation the output power by the phase current maximal control. Obtaining the nominal power or greater in the CP range with the CC control causes a decrease of the efficiency of drive (Fig. 16). After adhibition of the motor in CC state, the general efficiency of the drive will be insignificantly decreasing given output power with increasing rotation speed. This especially applies to the situation when the motor works with nominal power or in the range of overload. Adhibition of the drive system in the state of the CC control overload is dependent on the limitations of the control method and coupling temperature tolerance.

6. Conclusions

In this paper, an analysis of the proposed method of constant power range extension is presented. Simultaneous control of the maximum current value, turn-on, and turn-off angle allows one to maintain the reference output power values in a wide range of speed. The maximum output power is limited by the maximum temperature of the stator winding and the power loss of the drive system. Theoretically, if the power loss is omitted, it is possible to obtain a CP/CT ratio equal to ten.

Laboratory tests confirmed an increase in the possible CP/CT ratio.

The CC control method is very sensitive to changing control parameters. In the range of CC control, the range of changing turn-on angle and dwell angle is small. It is advisable to use detection of the rotor position with higher resolution (minimum twice).

Widening the range of the CP/CT ratio causes an increase in the electromagnetic torque ripple and declining efficiency. It is possible to obtain a short-lived increase of the output power in the extensive range of rotation speed. Together with increasing the output power (especially above the nominal value), ones will be increasing. Adhibition of the motor in the CC state causes a decrease in the general efficiency of a drive system. For large values, the CP/CT ratio will be decreasing. It is possible to obtain an increase in output power (twice-time load) in a very wide

range of rotation speeds. However, this is connected with declining efficiency. Additionally, the motor can work in this state for only a few seconds.

Acknowledgments

This research was financed in part by the statutory funds (UPB) of the Department of Electrodynamics and Electrical Machine Systems, Rzeszow University of Technology and in the part by the Minister of Education and Science of the Republic of Poland within the "Regional Initiative of Excellence" program for the years 2019–2022. Project number 027/RID/2018/19, amount granted: 11 999 00 PLN. The article is a post-conference publication from the SME 2022 Electrical Machines Symposium.

References

[1] Agamloh E., von Jouanne A., Yokochi A., *An Overview of Electric Machine Trends in Modern Electric Vehicles*, Machines, vol. 8, no. 2, pp. 1–16 (2020), DOI: 10.3390/machines8020020.

[2] Yildirim M., Polat M., Kürüm H., *A survey on comparison of electric motor types and drives used for electric vehicles*, 16th International Power Electronics and Motion Control Conference and Exposition, pp. 218–223 (2014), DOI: 10.1109/EPEPEMC.2014.6980715.

[3] Pindoriya R.M., Rajpurohit B.S., Kumar R., Srivastava K.N., *Comparative analysis of permanent magnet motors and switched reluctance motors capabilities for electric and hybrid electric vehicles*, IEEMA Engineer Infinite Conference (eTechNxT), pp. 1–5 (2018), DOI: 10.1109/ETECHNXT.2018.8385282.

[4] Dutta R., Rahman M.F., *Design and Analysis of an Interior Permanent Magnet (IPM) Machine with Very Wide Constant Power Operation Range*, IEEE Transactions on Energy Conversion, vol. 23, no. 1, pp. 25–33 (2008), DOI: 10.1109/TEC.2007.905061.

[5] Bernard N., Dang L., Olivier J.C., Bracikowski N., Wasselynck G., Berthiau G., *Design Optimization of High-Speed PMSM for Electric Vehicles*, IEEE Vehicle Power and Propulsion Conference (VPPC), pp. 1–6 (2015), DOI: 10.1109/VPPC.2015.7352927.

[6] Liu X., Chen H., Zhao J., Belahcen A., *Research on the Performances and Parameters of Interior PMSM Used for Electric Vehicles*, IEEE Transactions on Industrial Electronics, vol. 63, no. 6, pp. 3533–3545 (2016), DOI: 10.1109/TIE.2016.2524415.

[7] Chau K.T., Chan C.C., Liu C., *Overview of Permanent-Magnet Brushless Drives for Electric and Hybrid Electric Vehicles*, IEEE Transactions on Industrial Electronics, vol. 55, no. 6, pp. 2246–2257 (2008), DOI: 10.1109/TIE.2008.918403.

[8] Hashemnia N., Asaei B., *Comparative study of using different electric motors in the electric vehicles*, 18th International Conference on Electrical Machines, pp. 1–5 (2008), DOI: 10.1109/ICELMACH.2008.4800157.

[9] Park H., Lim M., *Design of High Power Density and High Efficiency Wound-Field Synchronous Motor for Electric Vehicle Traction*, IEEE Access, vol. 7, pp. 46677–46685 (2019), DOI: 10.1109/ACCESS.2019.2907800.

[10] Schofield N., Long S.A., Howe D., McClelland M., *Design of a Switched Reluctance Machine for Extended Speed Operation*, IEEE Transactions on Industry Applications, vol. 45, no. 1, pp. 116–122 (2009), DOI: 10.1109/TIA.2008.2009506.

[11] Bertoluzzo M., Buja G., *Development of Electric Propulsion Systems for Light Electric Vehicles*, IEEE Transactions on Industrial Informatics, vol. 7, no. 3 (2011), DOI: 10.1109/TII.2011.2158840.

[12] Cai W., *Comparison and Review of Electric Machines for Integrated Starter Alternator Applications*, Conference Record of the 2004 IEEE Industry Applications Conference, 39th IAS Annual Meeting (2004), DOI: 10.1109/IAS.2004.1348437.

[13] Zaghari B., Stuikys A., Weddell A.S., Beeby S., *Efficient Energy Conversion in Electrically Assisted Bicycles Using a Switched Reluctance Machine Under Torque Control*, IEEE Access, vol. 20 (2020)

[14] Howey B., Bilgin B., Emadi A., *Design of an External-Rotor Direct Drive E-Bike Switched Reluctance Motor*, IEEE Transactions on Vehicular Technology, vol. 69, no. 3 (2020), DOI: 10.1109/TVT.2020.2965943.

[15] Moore S.W., Rahman K.M., Ehsani M., *Effect on Vehicle Performance of Extending the Constant Power Region of Electric Drive Motors*, SAE Technical Papers Series 1999-01–1152 (1999), DOI: 10.4271/1999-01-1152.

[16] 16 Miller T.J.E., *Electronic Control of Switched Reluctance Machines*, Newnes (2001)

[17] Yoopakdee C., Fuengwarodsakul N.H., *Experimental investigation of control parameters of SRM drive in continuous conduction mode*, 2015 18th International Conference on Electrical Machines and Systems (ICEMS), pp. 898–903 (2015), DOI: 10.1109/ICEMS.2015.7385162.

[18] Hannoun H., Hilairet M., Marchand C., *Experimental Validation of a Switched Reluctance Machine Operating in Continuous-Conduction Mode*, IEEE Transactions on Vehicular Technology, vol. 60, no. 4, pp. 1453–1460 (2011), DOI: 10.1109/TVT.2011.2124478.

[19] Korkosz M., Mazur D., *Operation of the switched reluctance motor at continuous conduction of phase current*, 2006 IEEE Mediterranean Electrotechnical Conference, pp. 1166–1169 (2006), DOI: 10.1109/MELCON.2006.1653308.

[20] Chiba A., Takeno M., Hoshi N., Takemoto M., Ogasawara S., Rahman M.A., *Consideration of Number of Series Turns in Switched-Reluctance Traction Motor Competitive to HEV IPMSM*, IEEE Transactions on Industry Applications, vol. 48, no. 6, pp. 2333–2340 (2012), DOI: 10.1109/TIA.2012.2227093.

[21] 21 Kiyota K., Chiba A., *Design of Switched Reluctance Motor Competitive to 60-kW IPMSM in Third-Generation Hybrid Electric Vehicle*, IEEE Transactions on Industry Applications, vol. 48, no. 6, pp. 2303–2309 (2012), DOI: 10.1109/TIA.2012.2227091.

[22] Bogusz P., Korkosz A., Powrózek A., *Analysis of mutual couplings influence on properties of the switched reluctance machine*, Przegląd Elektrotechniczny (in Polish), vol. 91, no. 8, pp. 139–142 (2015), DOI: 10.15199/48.2015.08.33.